THE JOURNAL OF PHYSICAL CHEMISTRY C
A JOURNAL OF THE AMERICAN CHEMICAL SOCIETY

pubs.acs.org/JPCC
Article

Assessing the Stability of Metal−Organic Frameworks with Local Vibrational Mode Theory

Sophia Trejo, Juliana J. Antonio, Elfi Kraka, and Haoyuan Chen*

Cite This: J. Phys. Chem. C 2026, 130, 2847−2854
Read Online

ACCESS | Metrics & More | Article Recommendations | Supporting Information

ABSTRACT: The stability of metal−organic frameworks (MOFs) is crucial for their industrial applications, with metal−linker coordination bonds often being the weakest structural points. Here, we assessed the strength of these bonds in representative MOF series (UiO-66, MOF-5, and ZIFs) using local vibrational mode theory, which converts delocalized normal modes to local vibrational modes and associated local mode force constants, reflecting bond strength. Good agreement between the bond strengths obtained from local force constants and the corresponding experimental stability data was obtained, which in some cases was not reflected by the electron density at the bond critical points. The effects of linker functionalization were also analyzed, in which *ortho*-NH_2 substitutions on the linkers were found to weaken the adjacent coordination bonds via intramolecular hydrogen bonding. These findings establish a readily computable quantum-mechanical metric for evaluating bond strengths in MOFs, paving the way for accurate evaluation and prediction of MOF stability.

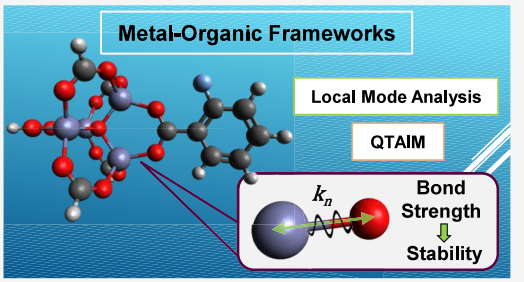

INTRODUCTION

Metal−organic frameworks (MOFs), a diverse class of crystalline nanoporous materials composed of inorganic nodes bridged by organic linkers, are characterized by their high surface areas, excellent tunability, and broad application potential in gas adsorption/separation, catalysis, and energy storage.[1−5] A fundamental requirement across these applications is structural stability, where MOFs must retain their framework integrity under chemical, thermal, and/or mechanical stress to remain functional in practical environments.[6] Despite many highly stable MOFs being synthesized, the factors that determine a MOF's stability are not fully understood.[6] Experimental techniques such as thermogravimetric analysis,[7,8] variable-temperature powder X-ray diffraction,[9] and surface area determination[10] can provide key insights into how these materials degrade or transform under operating conditions. Infrared spectroscopy, mass spectrometry, and electron microscopy offer complementary views into the chemical and morphological changes that accompany degradation.[11−14] While these methods provide valuable insights, they typically assess stability through macroscopic or bulk properties, which can disguise underlying electronic features such as bond strength and/or coordination environment. The coordination bonds that connect inorganic nodes and organic linkers are often regarded as the weakest links in MOF structures that limit the stability of MOFs. In most cases, MOF degradation—whether thermal, mechanical, or chemical—involves the breaking of coordination bonds.[6] Subtle variations in local bonding interactions that are not captured by global structural metrics can thus have a critical influence on the stability and performance of the materials.

To bridge this gap, computational approaches have emerged in dissecting the structural and bonding features of MOFs. Density functional theory (DFT) calculations and molecular dynamics simulations have been employed to study node−linker energetics, framework flexibility, and bond dissociation mechanisms.[15−18] However, quantifying bond strengths in a chemically transferable and physically rigorous manner remains challenging. For example, bond strengths are traditionally evaluated via the bond dissociation energy (BDE), which is the amount of energy necessary to homolytically cleave the bond. Even so, the cleavage of metal−linker (M−L) coordination bonds in MOFs is usually heterolytic and is often accompanied by solvent addition, which makes BDE not directly applicable as an intrinsic bond strength measure.

To overcome these limitations, we applied local vibrational mode analysis, which provides bond-specific local force constants that can be directly related to bond strength. Unlike conventional vibrational analyses which generate canonical normal modes that are often delocalized, local mode theory provides a bond strength measure associated with individual bonds, making it particularly suited for chemically diverse systems. Previous investigations employing local mode analysis (LMA) have shown its effectiveness in quantifying metal−

Received: January 20, 2026
Revised: January 28, 2026
Accepted: January 30, 2026
Published: February 3, 2026

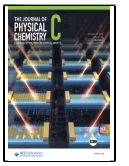

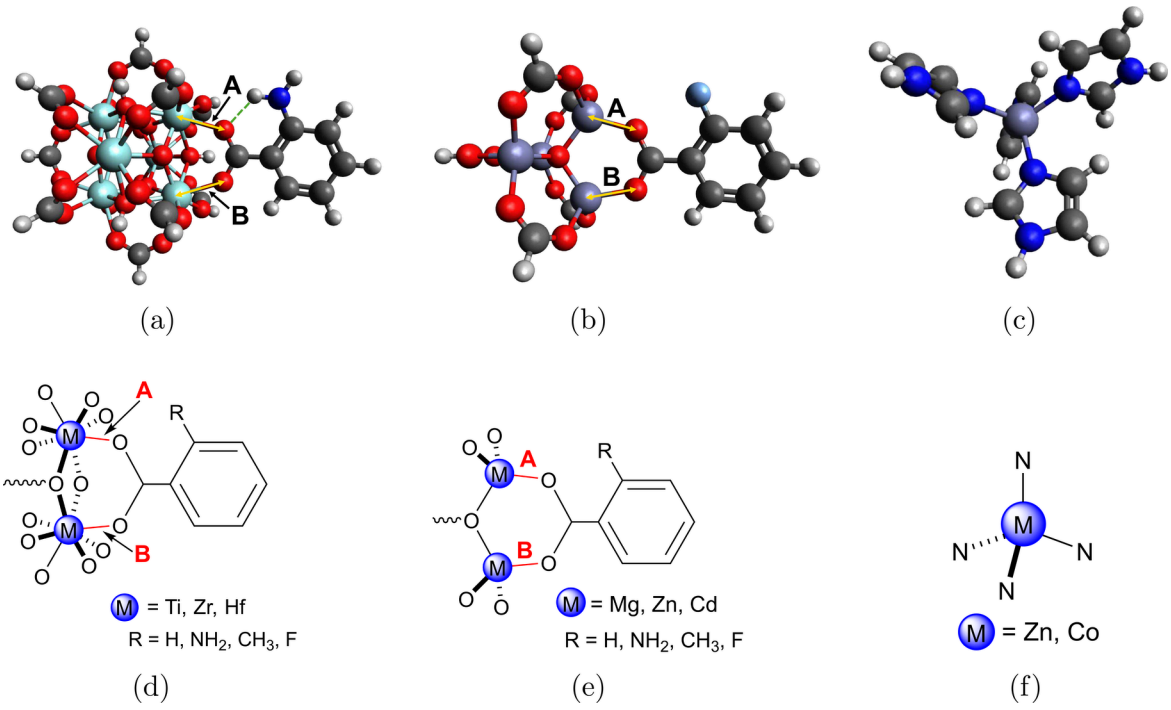

Figure 1. Representative molecular models from the three MOF series studied in this work: (a) Zr-UiO-66 (linker functionalized with $-NH_2$), (b) Zn-MOF-5 (linker functionalized with −F), (c) ZIF-4 and structural motifs for (d) UiO-66 series, (e) MOF-5 series, and (f) ZIF series. The "A" or "B" labels denote metal−linker coordination bonds that are adjacent to or away from the functional group on the linker, respectively. Color codes: H, white; C, gray; N, blue; O, red; F, light blue; Zn, violet; Zr, cyan.

ligand bond strengths across diverse coordination environments.[19,20] In this work, we performed a comparative LMA on cluster models of three representative families of MOFs as shown in Figure 1: UiO-66-series, MOF-5-series, and ZIF-series, featuring a variety of metal centers and functionalized linkers. Our objective was to evaluate the utility and transferability of the local bond stretching force constant as a quantitative descriptor of the M−L bond strength in MOFs. By comparing with conventional structural and electronic metrics such as bond lengths, bond orders, and electron density at bond critical points (BCPs) (ρ_b) derived from the quantum theory of atoms in molecules (QTAIM),[21] we could quantify utilizing the various descriptors and provide new insights into the chemical factors that contribute to MOF stability at the atomic level.

METHODOLOGY

Three representative types of MOFs and their respective variations featuring M−L coordination bonds were studied: UiO-66[22−24] (M = Ti, Zr, and Hf), MOF-5[25] (M = Mg, Zn, and Cd), and zeolitic imidazolate frameworks[26,27] (ZIF-4, ZIF-7, ZIF-8, and ZIF-67; M = Zn and Co). For the UiO-66 and MOF-5 series, functional groups ($-NH_2$, $-CH_3$, and −F) were also considered at the *ortho*-position on the organic linkers. The UiO-66 series also include the recently reported phosphonate-based MOFs NU-406 and NU-407[28] (M = Zr) which have the same inorganic node and topology as UiO-66. In addition, the mixed-linker MOF DMOF-1[29] (M = Zn) featuring both Zn−O and Zn−N coordination bonds was studied as a test case in which the strengths of the two bonds were compared against each other.

The molecular structures were initially obtained from crystal structures[26,28,29] and previous works,[30,31] followed by geometry optimizations at the M06-L[32]/def2-SVP[33,34] level. Since the implementation of def2-SVP in Gaussian16 is all-electron for H−Kr and has SDD[35] effective core potential (ECP) for Kr and beyond, we manually applied the SDD ECP for Ti, Fe, Co, and Zn to ensure methodological consistency. Harmonic vibrational frequency calculations for the optimized structures were then performed using the same level of theory. Both geometry optimizations and frequency calculations were performed in Gaussian16.[36] The LModeA2025 program[37] was then used to extract local vibrational modes from the normal modes. All frequency calculations confirmed the optimized structures to be at a local minimum.

A brief overview of local vibrational mode theory is provided here, while readers interested in more details are referred to recent review articles.[38,39] Normal vibrational modes are typically delocalized in polyatomic systems, as first noted by Wilson in 1941.[40] This delocalization raises concerns about the reliability of using associated normal mode stretching force constants as indicators of bond strength. In contrast, local vibrational stretching force constants derived from local vibrational modes directly reflect the intrinsic strength of individual chemical bonds.

The local vibrational mode vector $\mathbf{a}_n$, is defined as[38,39]

$$\mathbf{a}_n = \frac{\mathbf{K}^{-1}\mathbf{d}_n^{\dagger}}{\mathbf{d}_n\mathbf{K}^{-1}\mathbf{d}_n^{\dagger}} \tag{1}$$

where $\mathbf{K}$ is the diagonal force constant matrix in normal mode coordinate $\mathbf{Q}$, and $\mathbf{d}_n$ denotes the n-th normal mode vector expressed in internal coordinates $\mathbf{q}$. Both quantities are readily available from a standard normal-mode analysis performed by most modern quantum chemistry software packages.[41] As a result, LMA can be carried out with minimal additional computational effort. For each local mode $\mathbf{a}_n$, the correspond-

https://doi.org/10.1021/acs.jpcc.6c00408
J. Phys. Chem. C 2026, 130, 2847−2854

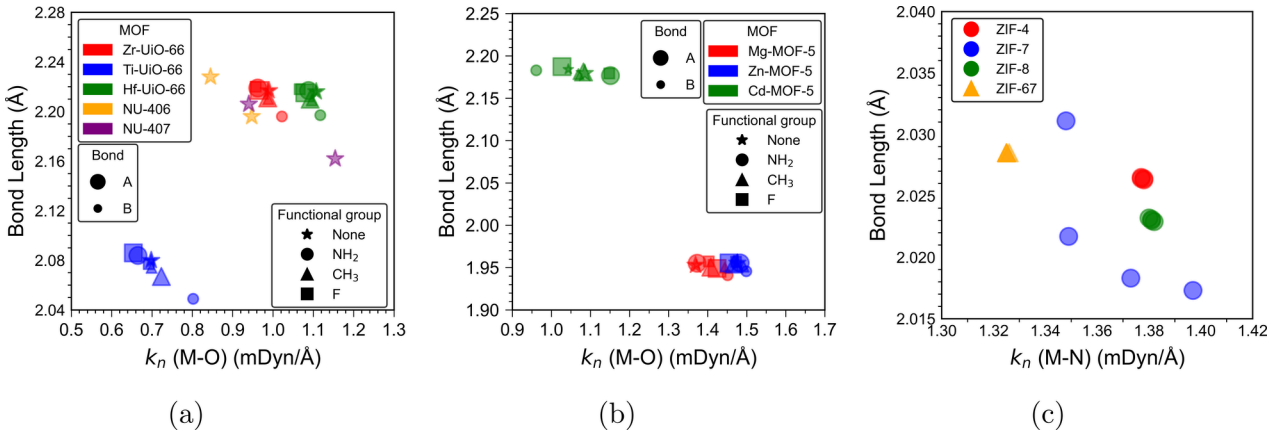

Figure 2. Bond length (Å) and k_n (mdyn/Å) of (a) UiO-66 series (including NU-406 and NU-407), (b) MOF-5 series, and (c) ZIF series.

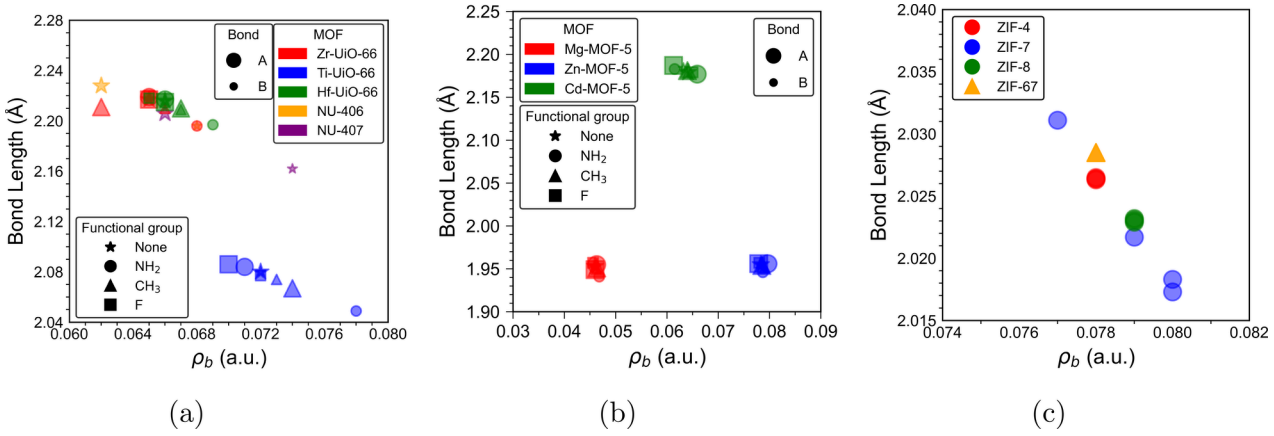

Figure 3. Bond length (Å) and ρ_b (a.u.) of (a) UiO-66 series (including NU-406 and NU-407), (b) MOF-5 series, and (c) ZIF series.

ing local force constant k_n, which characterizes the localized vibration of a given fragment (such as a bond stretching, bond angle bending, dihedral angle torsion, etc.), is defined as

$$k_n = \mathbf{a}_n^{\dagger}\mathbf{K}\mathbf{a}_n \tag{2}$$

Additional local mode properties, such as local vibrational frequencies and intensities, can be derived as well.[38,39]

The use of relative bond strength order (BSO n) is convenient when comparing a relatively large set of k_n values. According to the generalized Badger rule derived by Cremer, Kraka, and co-workers,[42] k_n and BSO n are related by a power relationship BSO $n = a(k_n)^b$. The constants a and b are determined by two reference compounds with known BSO n and k_n values, the constraint being that for a zero-force constant BSO n equals zero. To characterize M−L interactions, Fe−H and Fe═O were selected as reference molecules,[43−47] yielding values of a = 0.7513 and b = 0.4715. Notably, we employed scaled Mayer bond orders[48−50] as a more accurate reference for BSO n, where Fe−H is scaled to BSO n = 1 as a single bond (k_n = 1.834 mDyn/Å) and Fe═O is scaled to 1.71 (k_n = 5.690 mDyn/Å).

Establishing a comparison between k_n and ρ_b was also essential, as ρ_b has historically been widely related to the bond order, which has been used as an indicator of bond strength.[21,51] To evaluate the consistency between local force constants and QTAIM-based indicators of bonding, ρ_b values of all the M−L bonds were computed using the wavefunction analysis program Multiwfn3.8.[52−54]

RESULTS/DISCUSSION

Trends in Bond Length, k_n, and ρ_b

We begin by analyzing the general trends in bond length, k_n, and ρ_b for the three MOF series, as shown in Figure 2 and Figure 3. For the UiO-66 series (Figure 2a and Table 1), which only includes Group IV metals (Ti, Zr, Hf), the k_n values display an order of Ti < Zr ∼ Hf, indicating that the M−O bond strength in UiO-66 follows the same order. Interestingly, this order occurs despite an increase in bond length from Ti to Hf, which is likely a result of the increase in atomic radius. Experimentally, both Zr- and Hf-UiO-66 have been reported as highly stable MOFs with similar stability,[55] while Ti could only be introduced in UiO-66 via post-synthetic exchange which resulted in a mix-metal MOF.[56] Ti-carboxylate MOFs are more rarely seen in the literature compared to Zr-carboxylate ones in general.[56] These experimental observations suggest that Ti−O bonds are weaker than Zr−O and Hf−O bonds in UiO-66, which is consistent with our k_n values. Although bond length is often used as a gauge of bond strength, prior studies have shown that the relationship between bond length and bond strength is not consistently held, and a stronger bond does not always correlate with a shorter bond.[57,58] In this case, the local force constants, being sensitive to the overall electronic structure, quantify the intrinsic strength of the M−O stretching interaction. In comparison, ρ_b (Figure 3) follows the trend Ti > Zr ∼ Hf.

https://doi.org/10.1021/acs.jpcc.6c00408
J. Phys. Chem. C 2026, 130, 2847−2854

Table 1. Local mode (M−O), Bond Length (BL, Å), k_n (mDyn/Å), BSO ρ_b (a.u.), and $H(\mathbf{r})$ (Ha/Å^3) for UiO-66 Series[a]

UiO-66	Local Mode (M−O)	k_n(M−O)	BL	BSO	ρ_b	$H(\mathbf{r})$
Ti	A	0.698	2.080	0.634	0.072	−0.015
	B	0.698	2.080	0.634	0.072	−0.015
Ti_NH_2	A	0.665	2.084	0.620	0.071	−0.014
	B	0.802	2.049	0.677	0.078	−0.022
Ti_CH_3	A	0.723	2.067	0.645	0.074	−0.018
	B	0.699	2.074	0.635	0.073	−0.017
Ti_F	A	0.654	2.086	0.615	0.070	−0.013
	B	0.692	2.077	0.632	0.072	−0.015
Zr	A	0.990	2.217	0.748	0.065	−0.002
	B	0.990	2.217	0.748	0.065	−0.002
Zr_NH_2	A	0.962	2.219	0.738	0.065	−0.002
	B	1.022	2.196	0.759	0.068	−0.005
Zr_CH_3	A	0.987	2.211	0.747	0.062	−0.002
	B	0.988	2.210	0.747	0.066	−0.003
Zr_F	A	0.966	2.218	0.739	0.065	−0.000
	B	0.957	2.220	0.736	0.065	−0.001
Hf	A	1.107	2.216	0.788	0.066	0.003
	B	1.107	2.216	0.788	0.066	0.002
Hf_NH_2	A	1.088	2.217	0.782	0.066	0.002
	B	1.117	2.197	0.792	0.069	0.001
Hf_CH_3	A	1.092	2.210	0.783	0.067	0.002
	B	1.096	2.209	0.784	0.067	0.002
Hf_F	A	1.079	2.215	0.779	0.066	0.004
	B	1.066	2.218	0.774	0.065	0.003
NU-406	1	0.845	2.229	0.694	0.062	0.005
	2	0.947	2.196	0.732	0.068	−0.004
NU-407	1	0.940	2.206	0.730	0.066	−0.003
	2	1.154	2.162	0.804	0.074	−0.016

[a]A and B are defined in the main text. NU-406 and NU-407 have (Zr−O) local modes that are equivalent and are therefore labeled as 1 and 2.

For the MOF-5 series (Figure 2b, Figure 3b, and Table 2), which includes metals from different groups, the results were more complex. For the Group XII metals Zn and Cd, both k_n and ρ_b decreased as the bond length increased, suggesting that the Cd−O bond is weaker than the Zn−O bond in MOF-5. This is supported by the fact that the synthesis of Cd-MOF-5 has not been reported yet,[59] while Zn-MOF-5 was one of the earliest MOFs discovered.[25] For Mg, k_n from LMA suggested a bond strength similar to Zn−O, whereas ρ_b was much lower than Cd. A previous computational study reported that the formation energy of Mg-MOF-5 is more negative than Zn-MOF-5,[60] supporting the interpretation that k_n provides a reliable measure of strength in this series.

For the ZIF series (Figure 2c, Figure 3c, and Table 3), the bond lengths and k_n and ρ_b values for the Zn−N bonds (ZIF-4, ZIF-7, and ZIF-8) were all considerably close (note that the range of the k_n axis in Figure 2c is much narrower than in Figure 2a and Figure 2b), due to the similar chemical environment around those bonds. Nevertheless, both k_n and ρ_b suggested that the Zn−N bond is slightly stronger in ZIF-8 (when averaged, 1.381 mDyn/Å and 0.0791 a.u.) than in ZIF-7 (average of 1.366 mDyn/Å and 0.0789 a.u.), which is supported by the experimental finding that in boiling water ZIF-8 remained stable after 7 days while ZIF-7 transformed to another crystalline material after 1 day.[26] ZIF-67, which has the same structure as ZIF-8 except Zn^{2+} was replaced by Co^{2+}, has been shown to be less water-stable than ZIF-8.[61,62] Here, both ρ_b and LMA yielded slightly lower values for the Co−N bond in ZIF-67 compared to the Zn−N bond in ZIF-8. This is

Table 2. Local Mode (M−O), Bond Length (BL, Å), k_n (mDyn/Å), BSO, ρ_b (a.u.), and $H(\mathbf{r})$ (Ha/Å^3) for MOF-5 Series[a]

MOF-5	Local Mode (M−O)	k_n(M−O)	BL	BSO	ρ_b	$H(\mathbf{r})$
Mg	A	1.369	1.953	0.871	0.046	0.104
	B	1.371	1.953	0.872	0.046	0.104
Mg_NH_2	A	1.373	1.955	0.872	0.046	0.102
	B	1.451	1.941	0.895	0.047	0.110
Mg_CH_3	A	1.408	1.951	0.883	0.046	0.105
	B	1.444	1.950	0.893	0.046	0.106
Mg_F	A	1.424	1.949	0.888	0.046	0.107
	B	1.403	1.957	0.881	0.046	0.102
Zn	A	1.476	1.955	0.903	0.078	0.027
	B	1.476	1.955	0.903	0.078	0.027
Zn_NH_2	A	1.483	1.956	0.905	0.080	0.028
	B	1.499	1.946	0.909	0.079	0.026
Zn_CH_3	A	1.467	1.954	0.900	0.078	0.027
	B	1.492	1.951	0.907	0.079	0.027
Zn_F	A	1.455	1.956	0.897	0.078	0.029
	B	1.473	1.957	0.902	0.078	0.027
Cd	A	1.085	2.179	0.781	0.064	0.002
	B	1.043	2.184	0.766	0.063	0.003
Cd_NH_2	A	1.151	2.177	0.803	0.066	−0.003
	B	0.961	2.183	0.737	0.061	0.009
Cd_CH_3	A	1.082	2.181	0.780	0.064	0.002
	B	1.069	2.179	0.775	0.064	0.004
Cd_F	A	1.027	2.187	0.761	0.061	0.008
	B	1.148	2.179	0.802	0.065	−0.001

[a]For the local mode, A and B are referenced in the main text.

Table 3. Local Mode (M−N), Bond Length (BL, Å), k_n (mDyn/Å), BSO, ρ_b (a.u.), and $H(\mathbf{r})$ (Ha/Å^3) for ZIF Series[a]

ZIF	Local Mode (Zn−N)	k_n(Zn−N)	BL	BSO	ρ_b	$H(\mathbf{r})$
ZIF-4	1	1.377	2.027	0.874	0.078	−0.031
	2	1.377	2.026	0.874	0.078	−0.031
	3	1.378	2.026	0.874	0.078	−0.031
	4	1.378	2.026	0.874	0.078	−0.031
ZIF-7	1	1.349	2.022	0.865	0.079	−0.034
	2	1.348	2.031	0.865	0.077	−0.030
	3	1.397	2.017	0.880	0.080	−0.035
	4	1.373	2.018	0.872	0.080	−0.034
ZIF-8	1	1.380	2.023	0.875	0.079	−0.035
	2	1.382	2.023	0.875	0.079	−0.035
	3	1.381	2.023	0.875	0.079	−0.035
	4	1.381	2.023	0.875	0.079	−0.035
ZIF	Local Mode (Co−N)	k_n(Co−N)	BL	BSO	ρ_b	$H(\mathbf{r})$
ZIF-67	1	1.326	2.029	0.858	0.078	−0.022
	2	1.325	2.029	0.858	0.078	−0.022
	3	1.325	2.029	0.858	0.078	−0.022
	4	1.325	2.029	0.858	0.078	−0.022

[a]All four local modes are equivalent in each ZIF and are labeled as numbers 1−4.

https://doi.org/10.1021/acs.jpcc.6c00408
J. Phys. Chem. C 2026, 130, 2847−2854

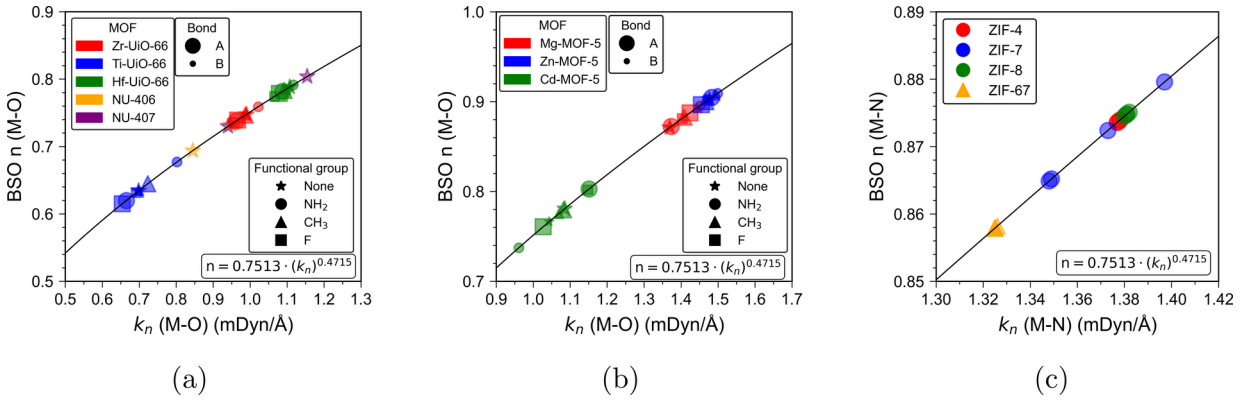

Figure 4. BSO and k_n (mDyn/Å) for (a) UiO-66 series (including NU-406 and NU-407), (b) MOF-5 series, and (c) ZIF series. (a) and (b) series also include functionalized versions. "A" and "B" are defined in Figure 1.

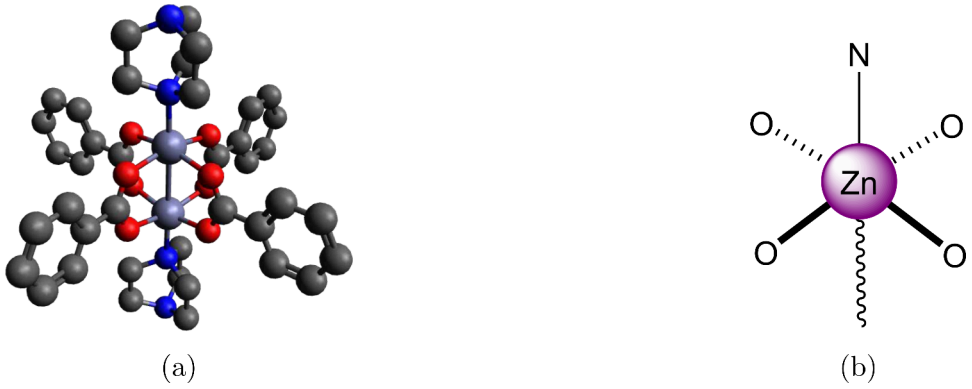

Figure 5. (a) Molecular model of DMOF-1 and (b) structural motif of the Zn center in DMOF-1. For visual clarity, hydrogen atoms have been omitted from the figure. Color codes: C, gray; N, blue; O, red; Zn, violet.

consistent with experimental observations. For k_n, the weakest bond comes from the ZIF-67 structure (Co−N), whereas for p_b, the weakest bond comes from the ZIF-7 (Zn−N) structure.

Trends in Functionalization

To enable comparison of bond strengths across chemically distinct systems and the effects of functionalization on M−L bonds, we applied the generalized Badger rule to transform local force constants k_n into relative bond orders BSO n. All BSO n values are between 0.65 and 1.0, identifying all M−L coordination bonds relatively close to a single bond. For the UiO-66 series (Figure 4a), the Ti (blue), Zr (red), and Hf (green) points formed three clusters from bottom left to top right, which showed that even with linker functionalizations the aforementioned trend in bond strengths still held. The two points for the Zr-phosphonate MOFs NU-406 (yellow) and NU-407 (purple), despite being slightly away from the cluster of Zr points (red), are still to the right of all Ti points (blue), emphasizing the strong impact of metal identity on the M−L bond strength. It is noteworthy that NU-407 was reported to have higher hydrolytic stability than NU-406,[28] which agrees with our results. Note that although the data in Figure 4a might look like linear correlation between k_n and BSO n it is actually a power−law relationship, as discussed earlier in the Methodology section.

Similarly, for the MOF-5 series (Figure 4b), three distinct clusters based on metal identity were observed. As discussed above, when going down the periodic table, the Zr−O bond was stronger than Ti−O; however, in this scenario, the Cd−O bond became weaker than Zn−O. This can be qualitatively rationalized by the hard and soft acid−base (HSAB) theory,[62,63] in which carboxylate is characterized as a hard base, Zn^{2+} as an acid of intermediate hardness, and Cd^{2+} as a soft acid. This is a possible explanation for the decrease in bond strength from Zn-MOF-5 to Cd-MOF-5. For the ZIF-series (Figure 4c), most points of Zn−N were very close together (note the axis ranges again), while the points corresponding to the Co−N bond and one of the Zn−N bonds from ZIF-7 (yellow triangle and blue circle) are separated.

Concerning the effects of linker functionalization, all UiO-66 MOFs (Figure 4a) functionalized with an *ortho*-NH_2 group on the linker (Figure 1a) had weaker A bond (large circles) and stronger B bond (small circles), compared to their respective unfunctionalized models (stars). This is due to intramolecular hydrogen bonding between the $-NH_2$ group and the O atom of M−O, which weakens the adjacent A bond by decreasing the electron density on the O atom. These findings are in agreement with experimental studies reporting a decrease in water stability in $-NH_2$-functionalized UiO-66.[62] $-CH_3$ and −F functionalizations do not display a clear trend across different MOFs. For the MOF-5 series (Figure 4b), $-NH_2$ functionalization exhibited slightly larger BSO value for bond B compared to bond A in the Mg and Zn models, consistent with the trend observed in UiO-66. However, Cd-MOF-5 exhibits an opposite trend where bond A becomes stronger than bond B, and the reason remains unclear. Overall, as mentioned above, the metal identity has a significantly larger impact than linker functionalization on the M−L bond strength.

https://doi.org/10.1021/acs.jpcc.6c00408
J. Phys. Chem. C 2026, 130, 2847−2854

To investigate the nature of the M−L bonds in the MOFs, we applied the Cremer−Kraka criterion[64] to assess the covalency of the bonds, in which the sign of the energy density ($H(\mathbf{r})$) at the bond critical point can indicate whether the bond is covalent ($H(\mathbf{r}) < 0$) or noncovalent/ionic ($H(\mathbf{r}) > 0$) (Supporting Information, Figures S4−S7). We found that in general $H(\mathbf{r})$ for most of the bonds is close to zero ($\sim 10^{-2}$ Ha/Å^3), indicating partial covalent and partial ionic characters. The only bond that exhibits significant ionic character is Mg−O in Mg-MOF-5 (Figure S4), which is the sole bond examined in this work that does not contain a transition metal. Within the UiO-66 series, an inverse correlation between k_n and $H(\mathbf{r})$ is observed (Figure S5), indicating that the stronger bonds are more covalent (except for Hf, where it has slight electrostatic character, despite being a stronger Hf−O bond). Another correlation is observed in ZIFs, where the stronger Zn−N bonds showed higher covalency than the weaker Co−N bond (Figure S7).

To further test the applicability of LMA, we selected DMOF-1[29] in which each Zn coordinates to both O and N (Figure 5). The Zn−N bonds in DMOF-1 have an average k_n of 1.11 mDyn/Å, revealing significantly weaker bond strengths than the Zn−N bonds in ZIFs (about 1.38 mDyn/Å). The Zn−O bonds in DMOF-1 (average k_n of 0.74 mDyn/Å) are considerably weaker than those in Zn-MOF-5 (about 1.48 mDyn/Å). The repulsion between the four oxygen atoms in the same plane in DMOF-1 might also be a reason why Zn−O bonds are weaker than Zn−N bonds despite being more electrostatically favorable. When looking at the $H(\mathbf{r})$ of these bonds (Table 4), the stronger Zn−N bonds show greater covalent character than the Zn−O bonds, which is consistent with the trend we observed in ZIFs. Our finding that Zn−N is stronger than Zn−O is also supported by a recent work,[65] which utilized a neural network model trained with extensive *ab initio* molecular dynamics data.

Table 4. Local Mode (Zn−N and Zn−O), Bond Length (BL, Å), k_n (mDyn/Å), BSO, ρ_b (a.u.), and $H(\mathbf{r})$ (Ha/Å^3) for DMOF-1[a]

Local Mode (Zn−N)	k_n(Zn−N)	BL	BSO	ρ_b	$H(\mathbf{r})$
1	1.111	2.090	0.790	0.070	−0.027
2	1.110	2.090	0.789	0.070	−0.027
Local Mode (Zn−O)	k_n(Zn−O)	BL	BSO	ρ_b	$H(\mathbf{r})$
1	0.740	2.061	0.652	0.063	0.017
2	0.730	2.065	0.648	0.062	0.016
3	0.715	2.066	0.641	0.062	0.016
4	0.774	2.055	0.666	0.063	0.017
1	0.756	2.061	0.658	0.063	0.017
2	0.713	2.065	0.641	0.062	0.016
3	0.772	2.056	0.665	0.063	0.017
4	0.724	2.067	0.645	0.062	0.016

[a]Both Zn−N bonds are equivalent and are labeled as 1 and 2. Each Zn atom in DMOF-1 is bonded to four equivalent oxygen atoms and are labeled as 1−4.

CONCLUSION

In conclusion, we demonstrated in this work that local bond stretching force constants k_n obtained from local vibrational mode theory provide a chemically meaningful and applicable measure of M−L bond strength in MOFs. In various MOF series, trends of k_n were able to explain known experimental findings on MOF stability. Comparisons between k_n and ρ_b reveal that these descriptors can exhibit different trends, as observed for the M−O bonds in UiO-66 and MOF-5, while yielding more comparable trends for the M−N bonds in ZIFs. It is important to note that these bond-strength descriptors alone are not sufficient to fully determine MOF stability, which also depends on collective structural and electronic factors at the framework level. It was also shown that metal identity has a greater impact on the M−L bond strength than linker functionalization. For DMOF-1, k_n predicted the same relative strength of Zn−N and Zn−O bonds as *ab initio* molecular dynamics simulations. Overall, this work establishes local vibrational mode theory as a robust and chemically insightful tool for assessing MOF stability, which can be integrated into high-throughput screening workflows as a quantitative descriptor to accelerate the discovery of functional MOF materials with desired stability.

ASSOCIATED CONTENT

Supporting Information

The Supporting Information is available free of charge at https://pubs.acs.org/doi/10.1021/acs.jpcc.6c00408.

Laplacian of electron density contour plots, energy density bar graph, and energy density vs local force constant (PDF)

Cartesian coordinates of all the optimized structures (ZIP)

AUTHOR INFORMATION

Corresponding Author

Haoyuan Chen − *Department of Chemistry, Southern Methodist University, Dallas, Texas 75275, United States;* orcid.org/0000-0002-8634-4028; Email: haoyuan@smu.edu

Authors

Sophia Trejo − *Department of Chemistry, Southern Methodist University, Dallas, Texas 75275, United States*

Juliana J. Antonio − *Department of Chemistry, Southern Methodist University, Dallas, Texas 75275, United States;* orcid.org/0000-0002-0358-9274

Elfi Kraka − *Department of Chemistry, Southern Methodist University, Dallas, Texas 75275, United States;* orcid.org/0000-0002-9658-5626

Complete contact information is available at: https://pubs.acs.org/10.1021/acs.jpcc.6c00408

Notes

The authors declare no competing financial interest.

ACKNOWLEDGMENTS

We acknowledge Southern Methodist University (SMU) O'Donnell Data Science and Research Computing Institute for computing resources. H.C. and S.T. acknowledge SMU for start-up funds. J.J.A. acknowledges the support from the National Science Foundation Graduate Research Fellowship Program under Grant No. DGE-2034834. S.T. acknowledges Ariel Trejo for helping with data visualization.

REFERENCES

(1) Freund, R.; Zaremba, O.; Arnauts, G.; Ameloot, R.; Skorupskii, G.; Dincă, M.; Bavykina, A.; Gascon, J.; Ejsmont, A.; Goscianska, J.; Kalmutzki, M.; Lächelt, U.; Ploetz, E.; Diercks, C. S.; Wuttke, S. The Current Status of MOF and COF Applications. *Angew. Chem., Int. Ed.* **2021**, *60*, 23975−24001.

(2) Zhou, H.-C.; Long, J. R.; Yaghi, O. M. Introduction to Metal−Organic Frameworks. *Chem. Rev.* **2012**, *112*, 673−674.

(3) Hou, C.-C.; Xu, Q. Metal−Organic Frameworks for Energy. *Adv. Energy Mater.* **2019**, *9*, 1801307.

(4) Lee, J.; Farha, O. K.; Roberts, J.; Scheidt, K. A.; Nguyen, S. T.; Hupp, J. T. Metal−organic framework materials as catalysts. *Chem. Soc. Rev.* **2009**, *38*, 1450−1459.

(5) Li, J.-R.; Sculley, J.; Zhou, H.-C. Metal−Organic Frameworks for Separations. *Chem. Rev.* **2012**, *112*, 869−932.

(6) Ding, M.; Cai, X.; Jiang, H.-L. Improving MOF stability: approaches and applications. *Chem. Sci.* **2019**, *10*, 10209−10230.

(7) Lázaro, I. A. A Comprehensive Thermogravimetric Analysis Multifaceted Method for the Exact Determination of the Composition of Multifunctional Metal-Organic Framework Materials. *Eur. J. Inorg. Chem.* **2020**, *2020*, 4284−4294.

(8) Jones, W. M.; Tapia, J. B.; Tuttle, R. R.; Reynolds, M. M. Thermogravimetric Analysis and Mass Spectrometry Allow for Determination of Chemisorbed Reaction Products on Metal Organic Frameworks. *Langmuir* **2020**, *36*, 3903−3911.

(9) Abid, H. R.; Azhar, M. R.; Iglauer, S.; Rada, Z. H.; Al-Yaseri, A.; Keshavarz, A. Physicochemical characterization of metal organic framework materials: A mini review. *Heliyon* **2024**, *10*, No. e23840.

(10) Sinha, P.; Datar, A.; Jeong, C.; Deng, X.; Chung, Y. G.; Lin, L.-C. Surface Area Determination of Porous Materials Using the Brunauer−Emmett−Teller (BET) Method: Limitations and Improvements. *J. Phys. Chem. C* **2019**, *123*, 20195−20209.

(11) Hadjiivanov, K. I.; Panayotov, D. A.; Mihaylov, M. Y.; Ivanova, E. Z.; Chakarova, K. K.; Andonova, S. M.; Drenchev, N. L. Power of Infrared and Raman Spectroscopies to Characterize Metal-Organic Frameworks and Investigate Their Interaction with Guest Molecules. *Chem. Rev.* **2021**, *121*, 1286−1424.

(12) Yang, S.-S.; Shi, M.-Y.; Tao, Z.-R.; Wang, C.; Gu, Z.-Y. Recent applications of metal−organic frameworks in matrix-assisted laser desorption/ionization mass spectrometry. *Anal. Bioanal. Chem.* **2019**, *411*, 4509−4522.

(13) Liu, L.; Zhang, D.; Zhu, Y.; Han, Y. Bulk and local structures of metal−organic frameworks unravelled by high-resolution electron microscopy. *Commun. Chem.* **2020**, *3*, 99.

(14) Zhu, Y.; Ciston, J.; Zheng, B.; Miao, X.; Czarnik, C.; Pan, Y.; Sougrat, R.; Lai, Z.; Hsiung, C.-E.; Yao, K.; Pinnau, I.; Pan, M.; Han, Y. Unravelling surface and interfacial structures of a metal−organic framework by transmission electron microscopy. *Nat. Mater.* **2017**, *16*, 532−536.

(15) Redfern, L. R.; Ducamp, M.; Wasson, M. C.; Robison, L.; Son, F. A.; Coudert, F.-X.; Farha, O. K. Isolating the Role of the Node-Linker Bond in the Compression of UiO-66 Metal−Organic Frameworks. *Chem. Mater.* **2020**, *32*, 5864−5871.

(16) Novendra, N.; Marrett, J. M.; Katsenis, A. D.; Titi, H. M.; Arhangelskis, M.; Friščić, T.; Navrotsky, A. Linker Substituents Control the Thermodynamic Stability in Metal−Organic Frameworks. *J. Am. Chem. Soc.* **2020**, *142*, 21720−21729.

(17) Yang, L.-M.; Vajeeston, P.; Ravindran, P.; Fjellvåg, H.; Tilset, M. Theoretical Investigations on the Chemical Bonding, Electronic Structure, And Optical Properties of the Metal-Organic Framework MOF-5. *Inorg. Chem.* **2010**, *49*, 10283−10290.

(18) Greathouse, J. A.; Allendorf, M. D. The Interaction of Water with MOF-5 Simulated by Molecular Dynamics. *J. Am. Chem. Soc.* **2006**, *128*, 10678−10679.

(19) Cremer, D.; Kraka, E. Generalization of the Tolman Electronic Parameter: The Metal-Ligand Electronic Parameter and the Intrinsic Strength of the Metal-Ligand Bond. *Dalton Trans.* **2017**, *46*, 8323−8338.

(20) Kraka, E.; Freindorf, M. In *Topics in Organometallic Chemistry - New Directions in the Modeling of Organometallic Reactions*; Lledós, A., Ujaque, G., Eds.; Springer: Berlin, Heidelberg, 2020; Vol. *67*, pp 1−43.

(21) Bader, R. F. W. *Atoms in Molecules: A Quantum Theory*; Clarendon Press: Oxford, 1995.

(22) Cavka, J. H.; Jakobsen, S.; Olsbye, U.; Guillou, N.; Lamberti, C.; Bordiga, S.; Lillerud, K. P. A New Zirconium Inorganic Building Brick Forming Metal Organic Frameworks with Exceptional Stability. *J. Am. Chem. Soc.* **2008**, *130*, 13850−13851.

(23) Jakobsen, S.; Gianolio, D.; Wragg, D. S.; Nilsen, M. H.; Emerich, H.; Bordiga, S.; Lamberti, C.; Olsbye, U.; Tilset, M.; Lillerud, K. P. Structural determination of a highly stable metal-organic framework with possible application to interim radioactive waste scavenging: Hf-UiO-66. *Phys. Rev. B* **2012**, *86*, 125429.

(24) Sun, D.; Liu, W.; Qiu, M.; Zhang, Y.; Li, Z. Introduction of a mediator for enhancing photocatalytic performance via post-synthetic metal exchange in metal−organic frameworks (MOFs). *Chem. Commun.* **2015**, *51*, 2056−2059.

(25) Rosi, N. L.; Eckert, J.; Eddaoudi, M.; Vodak, D. T.; Kim, J.; O'Keeffe, M.; Yaghi, O. M. Hydrogen Storage in Microporous Metal-Organic Frameworks. *Science* **2003**, *300*, 1127−1129.

(26) Park, K. S.; Ni, Z.; Côté, A. P.; Choi, J. Y.; Huang, R.; Uribe-Romo, F. J.; Chae, H. K.; O'Keeffe, M.; Yaghi, O. M. Exceptional chemical and thermal stability of zeolitic imidazolate frameworks. *Proc. Natl. Acad. Sci. U. S. A.* **2006**, *103*, 10186−10191.

(27) Banerjee, R.; Phan, A.; Wang, B.; Knobler, C.; Furukawa, H.; O'Keeffe, M.; Yaghi, O. M. High-Throughput Synthesis of Zeolitic Imidazolate Frameworks and Application to CO_2 Capture. *Science* **2008**, *319*, 939−943.

(28) Xie, H.; Kirlikovali, K. O.; Chen, Z.; Idrees, K. B.; Islamoglu, T.; Farha, O. K. A synthetic strategy towards single crystals of Zr_6 cluster and phosphonate-based metal−organic frameworks. *J. Mater. Chem. A* **2024**, *12*, 6399−6404.

(29) Dybtsev, D. N.; Chun, H.; Kim, K. Rigid and Flexible: A Highly Porous Metal−Organic Framework with Unusual Guest-Dependent Dynamic Behavior. *Angew. Chem., Int. Ed.* **2004**, *43*, 5033.

(30) Sillar, K.; Hofmann, A.; Sauer, J. Ab Initio Study of Hydrogen Adsorption in MOF-5. *J. Am. Chem. Soc.* **2009**, *131*, 4143−4150.

(31) Chen, H. Computational study of Brønsted acidity in the metal−organic framework UiO-66. *Chem. Phys. Lett.* **2022**, *800*, 139658.

(32) Zhao, Y.; Truhlar, D. G. A new local density functional for main-group thermochemistry, transition metal bonding, thermochemical kinetics, and noncovalent interactions. *J. Chem. Phys.* **2006**, *125*, 194101.

(33) Andrae, D.; Häußermann, U.; Dolg, M.; Stoll, H.; Preuß, H. Energy-adjustedab initio pseudopotentials for the second and third row transition elements. *Theor. Chim. Acta* **1990**, *77*, 123−141.

(34) Weigend, F.; Ahlrichs, R. Balanced basis sets of split valence, triple zeta valence and quadruple zeta valence quality for H to Rn: Design and assessment of accuracy. *Phys. Chem. Chem. Phys.* **2005**, *7*, 3297.

(35) Dolg, M.; Wedig, U.; Stoll, H.; Preuss, H. Energy-adjusted ab initio pseudopotentials for the first row transition elements. *J. Chem. Phys.* **1987**, *86*, 866−872.

(36) Frisch, M. J.; Trucks, G. W.; Schlegel, H. B.; Scuseria, G. E.; Robb, M. A.; Cheeseman, J. R.; Scalmani, G.; Barone, V.; Petersson, G. A.; Nakatsuji, H.; Li, X.; Caricato, M.; Marenich, A. V.; Bloino, J.; Janesko, B. G.; Gomperts, R.; Mennucci, B.; Hratchian, H. P.; Ortiz, J. V.; Izmaylov, A. F.; Sonnenberg, J. L.; Williams-Young, D.; Ding, F.; Lipparini, F.; Egidi, F.; Goings, J.; Peng, B.; Petrone, A.; Henderson, T.; Ranasinghe, D.; Zakrzewski, V. G.; Gao, J.; Rega, N.; Zheng, G.; Liang, W.; Hada, M.; Ehara, M.; Toyota, K.; Fukuda, R.; Hasegawa, J.; Ishida, M.; Nakajima, T.; Honda, Y.; Kitao, O.; Nakai, H.; Vreven, T.; Throssell, K.; Montgomery, J. A., Jr.; Peralta, J. E.; Ogliaro, F.; Bearpark, M. J.; Heyd, J. J.; Brothers, E. N.; Kudin, K. N.; Staroverov, V. N.; Keith, T. A.; Kobayashi, R.; Normand, J.; Raghavachari, K.; Rendell, A. P.; Burant, J. C.; Iyengar, S. S.; Tomasi, J.; Cossi, M.;

https://doi.org/10.1021/acs.jpcc.6c00408
J. Phys. Chem. C 2026, 130, 2847−2854

Millam, J. M.; Klene, M.; Adamo, C.; Cammi, R.; Ochterski, J. W.; Martin, R. L.; Morokuma, K.; Farkas, O.; Foresman, J. B.; Fox, D. J. *Gaussian 16 Revision*, C.02.; Gaussian Inc.: Wallingford CT, 2016.
(37) Zou, W.; Moura, R., Jr.; Santos, C. V., Jr.; Quintano, M.; Bodo, F.; Freindorf, M.; Cremer, D.; Kraka, E. *LModeA2025. Computational and Theoretical Chemistry Group (CATCO)*; Southern Methodist University: Dallas, TX, USA, 2025.
(38) Kraka, E.; Zou, W.; Tao, Y. Decoding Chemical Information from Vibrational Spectroscopy Data: Local Vibrational Mode Theory. *WIREs: Comput. Mol. Sci.* **2020**, *10*, 1480.
(39) Kraka, E.; Quintano, M.; La Force, H. W.; Antonio, J. J.; Freindorf, M. The Local Vibrational Mode Theory and Its Place in the Vibrational Spectroscopy Arena. *J. Phys. Chem. A* **2022**, *126*, 8781−8798.
(40) Wilson, E. B. Some Mathematical Methods for the Study of Molecular Vibrations. *J. Chem. Phys.* **1941**, *9*, 76−84.
(41) Barone, V.; Alessandrini, S.; Biczysko, M.; Cheeseman, J. R.; Clary, D. C.; McCoy, A. B.; DiRisio, R. J.; Neese, F.; Melosso, M.; Puzzarini, C. Computational molecular spectroscopy. *Nat. Rev. Methods Primers* **2021**, *1*, 38.
(42) Kraka, E.; Larsson, J. A.; Cremer, D. In *Computational Spectroscopy*; Grunenberg, J., Ed.; Wiley: New York, 2010; pp 105−149.
(43) Hendrickx, M.; Anam, K. A New Proposal for the Ground State of the FeO^- Cluster in the Gas Phase and for the Assignment of Its Photoelectron Spectra. *J. Phys. Chem. A* **2009**, *113*, 8746−8753.
(44) Bagus, P.; Preston, H. Lowest $^5\Sigma^+$ state of FeO: An *ab initio* investigation. *J. Chem. Phys.* **1973**, *59*, 2986−3002.
(45) Sodupe, M.; Lluch, J.; Olivia, A.; Illas, F.; Rubio, J. *Ab initio* study of the ground and low-lying states of FeH. *J. Chem. Phys.* **1990**, *92*, 2478−2480.
(46) Bauschlicher, C.; Langhoff, S. Theoretical confirmation of a $^4\delta$ ground state for FeH. *Chem. Phys. Lett.* **1988**, *145*, 205−210.
(47) Antonio, J. J.; Kraka, E. Non-covalent π−interactions in mutated aquomet-Myoglobin proteins: A QM/MM and Local Vibrational Mode Study. *Biochemistry* **2023**, *62*, 2325−2337.
(48) Mayer, I. Charge, bond brder an valence in the ab initio theory. *Chem. Phys. Lett.* **1983**, *97*, 270−274.
(49) Mayer, I. Bond orders and valences from ab initio wave functions. *Int. J. Quantum Chem.* **1986**, *29*, 477−483.
(50) Mayer, I. Bond order and valence indices: A personal account. *J. Comput. Chem.* **2007**, *28*, 204−221.
(51) Popelier, P. L. A. Characterization of a Dihydrogen Bond on the Basis of the Electron Density. *J. Phys. Chem. A* **1998**, *102*, 1873−1878.
(52) Lu, T.; Chen, F. Multiwfn: A multifunctional wavefunction analyzer. *J. Comput. Chem.* **2012**, *33*, 580−592.
(53) Lu, T. A comprehensive electron wavefunction analysis toolbox for chemists, Multiwfn. *J. Chem. Phys.* **2024**, *161*, 082503.
(54) Li, B.; Xu, H.; Dang, Y. Dispersion Interactions in Asymmetric Induction for Constructing Vicinal Stereogenic Centers. *Acc. Chem. Res.* **2023**, *56*, 3260−3270.
(55) Nord, M. T.; Plaman, A. S.; Zakharov, L. N.; Farha, O. K.; Nyman, M. Acid Stability of MIV (M = Zr, Hf, Ce, Th) UiO-66 MOFs from a Solution Perspective. *ACS Appl. Mater. Interfaces* **2025**, *17*, 21357−21370.
(56) Yuan, S.; Qin, J.-S.; Lollar, C. T.; Zhou, H.-C. Stable Metal−Organic Frameworks with Group 4 Metals: Current Status and Trends. *ACS Cent. Sci.* **2018**, *4*, 440−450.
(57) Kraka, E.; Cremer, D. Weaker Bonds with Shorter Bond Lengths. *Rev. Proc. Quim.* **2012**, *6*, 31−42.
(58) Kraka, E.; Setiawan, D.; Cremer, D. Re-Evaluation of the Bond Length-Bond Strength Rule: The Stronger Bond Is not Always the Shorter Bond. *J. Comput. Chem.* **2016**, *37*, 130−142.
(59) Yang, L.-M.; Ravindran, P.; Vajeeston, P.; Svelle, S.; Tilset, M. A quantum mechanically guided view of Cd-MOF-5 from formation energy, chemical bonding, electronic structure, and optical properties. *Microporous Mesoporous Mater.* **2013**, *175*, 50−58.
(60) Yang, L.-M.; Vajeeston, P.; Ravindran, P.; Fjellvåg, H.; Tilset, M. Revisiting isoreticular MOFs of alkaline earth metals: a comprehensive study on phase stability, electronic structure, chemical bonding, and optical properties of A−IRMOF-1 (A = Be, Mg, Ca, Sr, Ba). *Phys. Chem. Chem. Phys.* **2011**, *13*, 10191−10203.
(61) DelRe, C.; Hong, H.; Jiménez-Ángeles, F.; Wenny, M. B.; Erdosy, D. P.; Cho, J.; Britt, S.; Olvera de la Cruz, M.; Mason, J. A. Protein Coatings Dictate the Dispersibility and Stability of Hydrophobic Zeolitic-Imidazolate Frameworks in Water. *J. Phys. Chem. B* **2025**, *129*, 3120−3130.
(62) Yadav, A. K.; Kenny, M. S.; Musa, E. N.; Walz, T. J.; Gładysiak, A.; Stylianou, K. C. Hydrolytic Stability of Metal−Organic Frameworks: An Experimental Study. *Chem. Mater.* **2025**, *37*, 9965−9984.
(63) Pearson, R. G. Hard and Soft Acids and Bases. *J. Am. Chem. Soc.* **1963**, *85*, 3533−3539.
(64) Cremer, D.; Kraka, E. Chemical Bonds without Bonding Electron Density? Does the Difference Electron-Density Analysis Suffice for a Description of the Chemical Bond? *Angew. Chem., Int. Ed.* **1984**, *23*, 627−628.
(65) Chowdhury, R. A.; Ghose, B.; Choudhuri, D. Uncovering the Role of Critical Bonds in the Thermomechanical Response of Zn_2(1,4-benzenedicarboxylate)$_2$(1,4-diazabicyclo[2,2,2]octane) Using *Ab Initio* Simulations and Physics-Constrained Neural Networks. *Langmuir* **2025**, *41*, 12348−12364.

https://doi.org/10.1021/acs.jpcc.6c00408
J. Phys. Chem. C 2026, 130, 2847−2854